INTERNATIONAL ATOMIC ENERGY AGENCY
UNITED NATIONS EDUCATIONAL, SCIENTIFIC AND CULTURAL ORGANIZATION

INTERNATIONAL CENTRE FOR THEORETICAL PHYSICS
34100 TRIESTE (ITALY) - P.O.B. 586 - MIRAMARE - STRADA COSTIERA 11 - TELEPHONES: 224281/2/3/4/5/6
CABLE: CENTRATOM - TELEX 460392-1

SMR/115 - 9

WINTER COLLEGE ON LASERS, ATOMIC AND MOLECULAR PHYSICS

(21 January - 22 March 1985)

LASER PUMPING SYSTEMS

A. ANDREONI
Dipartimento di Fisica
Università degli Studi
Via Celoria, 16

20133 Milano
Italy

Principles of Lasers
SECOND EDITION

Orazio Svelto
Polytechnic Institute of Milan
Milan, Italy

Translated from Italian and edited by
David C. Hanna
Southampton University
Southampton, England

Plenum Press · New York and London

3
Pumping Processes

3.1 INTRODUCTION

We have seen in Chapter 1 that the process by which atoms are raised from level 1 to level 3 (for a three-level laser, Fig. 1.4a) or from level 0 to level 3 (for a four-level laser, Fig. 1.4b) is called the pumping process. Usually it is performed in one of the following two ways: optically or electrically. In *optical pumping* the light from a powerful source is absorbed by the active material and the atoms are thereby pumped into the upper pump level. This method is particularly suited to solid state (e.g., ruby or neodymium) and liquid (e.g., dye) lasers. The line broadening mechanisms in solids and liquids produce a very considerable broadening, so that usually one is dealing with pump bands rather than levels. These bands can, therefore, absorb a sizable fraction of the (usually broad-band) light emitted by the pumping lamp. *Electrical pumping* is accomplished by means of a sufficiently intense electrical discharge and is particularly suited to gas and semiconductor lasers. Gas lasers, in particular, do not usually lend themselves so readily to optical pumping because of the small widths of their absorption lines. On the other hand, semiconductor lasers can be optically pumped quite effectively, although electrical pumping is much more convenient. The two pumping processes mentioned above are not the only ones available for pumping lasers: For instance, pumping can also be achieved by a suitable chemical reaction (chemical pumping) or by a means of a supersonic gas expansion (gas-dynamic pumping). It should also be noted that, increasingly, lasers are being used for optical pumping of other lasers (solid-state, dye, and gas lasers). These latter pumping processes will

not be treated any further here and we refer the reader to Chapter 6 for further details.

If the pump level (or bands) are empty, the rate at which the upper state becomes populated by the pumping, $(dN_2/dt)_p$, is given by (1.10), where W_p is the pump rate. The purpose of this chapter is to give specific expressions for W_p, for both optical and electrical pumping.

3.2 OPTICAL PUMPING

Figure 3.1 is a schematic illustration of a quite general optical pumping system. The light from a powerful incoherent lamp is conveyed, by a suitable optical system, to the active material. The following two cases will be considered: (i) Pulsed lasers. In this case medium to high pressure (450–1500 Torr) Xe or Kr flashlamps are used. (ii) Continuous wave (cw) lasers. In this case high pressure (4000–8000 Torr) Kr or tungsten–iodine lamps are most often used. In case (i), the electrical energy stored in a capacitor bank is discharged into the flashlamp. The discharge is usually initiated by a high-voltage trigger pulse to an auxiliary electrode, and this pulse pre-ionizes the gas. The lamp then produces an intense flash of light whose duration (given by the product of storage capacitance and the lamp resistance) ranges from a few microseconds up to a few hundred microseconds. In both cases (i) and (ii), the active material is usually in the form of a cylindrical rod with a diameter ranging from a few millimeters up to a few centimeters and a length ranging from a few centimeters up to a few tens of centimeters.

Figure 3.2 shows three configurations which are particularly important examples of the general system sketched in Fig. 3.1.[1,2] In Figure 3.2a the lamp (usually a flashlamp) has a helical form, and the light reaches the active material either directly or after reflection at the specular cylindrical surface 1. This system was used for the first ruby laser, and it is still widely used for pulsed lasers. In Fig. 3.2b the lamp is in the form of a cylinder (linear lamp) of radius and length equal to those of the active rod. The

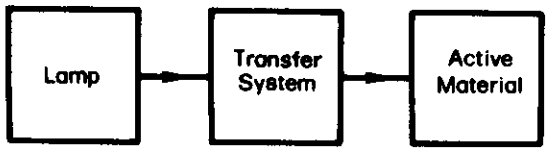

FIG. 3.1. General scheme of an optical pumping system.

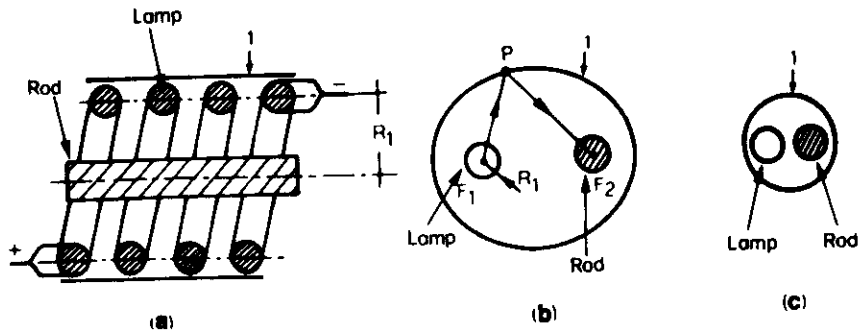

FIG. 3.2. Most commonly used optical pumping systems.

lamp is placed along one of the two focal axes, F_1, of a specularly reflecting elliptical cylinder (labeled 1 in the figure).[2] The laser rod is placed along the second focal axis F_2. A well-known property of an ellipse is that a ray F_1P leaving the first focus F_1 passes, after reflection by the elliptical surface, through the second focus F_2 (ray PF_2). This means that a large fraction of the light emitted by the lamp is conveyed, by reflection from the elliptical cylinder, to the active rod. Figure 3.2c shows what is called the close-coupling configuration. The rod and the linear lamp are placed as close as possible and are surrounded by a close-coupled cylindrical reflector (labeled 1 in the figure). The efficiency of the close-coupling configuration is usually not much lower than that of an elliptical cylinder. Note that cylinders made of diffusely reflecting material (such as compressed MgO or $BaSO_4$ powders or white ceramic) are sometimes used instead of the specular reflectors shown in Fig. 3.2. Although diffusive surfaces somewhat reduce the pump transfer efficiency, they have the advantage of providing a more uniform pumping of the active material. Multiple configurations using more than one elliptical cylinder or several lamps in close-coupling configurations have also been used. Figure 3.3 gives just two possible

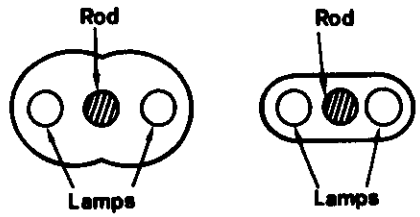

FIG. 3.3. Pump configurations using two lamps: (a) double-ellipse; (b) close-coupling.

examples. The efficiency of these multiple configurations is lower than for the corresponding single configurations of Fig. 3.2b and c. Nevertheless, they are often used in high-power (or high-energy) systems.

3.2.1. Pumping Efficiency

The overall pumping efficiency can be split up into three types of efficiency:

(i) *Transfer Efficiency* η_t, which is defined as the ratio of the pump power (or energy) actually entering the rod to the power (or energy) emitted by the lamp.

(ii) *Lamp Radiative Efficiency* η_r, which gives the efficiency of conversion of electrical input to light output in the wavelength range λ_1 to λ_2 in which the effective pump bands of the laser medium lie (e.g., 0.3 to 0.9 μm for Nd^{3+}:YAG). The lamp radiative efficiency is therefore given by

$$\eta_r = \frac{(2\pi Rl)\int_{\lambda_1}^{\lambda_2} I_\lambda \, d\lambda}{P} \tag{3.1}$$

where R is the radius and l the length of the lamp, I_λ is its spectral intensity, and P is the electrical power delivered to the lamp. Notice that, according to (3.1), I_λ can be written as

$$I_\lambda = \frac{P}{2\pi Rl}\eta_r g_\lambda \tag{3.2}$$

where g_λ is a normalized spectral intensity distribution (i.e., $\int_{\lambda_1}^{\lambda_2} g_\lambda \, d\lambda = 1$). Equation (3.2) allows one to calibrate I_λ once the uncalibrated spectrum of the emitted light and the lamp radiative efficiency η_r are known.

(iii) *Pump Quantum Efficiency* η_q, which accounts for the fact that not all of the atoms raised to the pump bands subsequently decay to the upper laser level. Some of these atoms can in fact decay from the pump bands straight back to the ground state or perhaps to other levels which are not useful. We will define the pump quantum efficiency $\eta_q(\lambda)$ as the ratio of the number of atoms which decay to the upper laser level to the number of atoms which are raised to the pump band by a monochromatic pump at wavelength λ.

The problem of improving the radiative efficiency is a challenging technical one for a lamp manufacturer. What are needed are lamps whose emission spectrum is a good match to the absorption spectrum of the pump bands. The quantum efficiency, on the other hand, is a quantity over which one can have little control since it depends on the properties of the given material. The transfer efficiency, however, depends a great deal on the

optical system chosen to convey the pump light to the laser rod. Its calculation is, therefore, important if one is to provide the optimum transfer conditions. The remainder of this section is devoted to this topic.

Before dealing with the calculation of the transfer efficiency, let us begin by finding a unified approach for analyzing the two pump configurations of Fig. 3.2a and b. Thus we shall assume that the pitch of the helix of Fig. 3.2a is very small. The presence of the reflecting cylindrical surface 1 allows us to represent the helical pumping system as shown schematically in Fig. 3.4a, where the shaded rod (lateral surface labeled S_2) is the laser rod and where the lamp is represented by the cylindrical surface S_1 having the same radius R_1 as the lamp radius (see Fig. 3.2a). In the case of Fig. 3.2b, all the rays emitted by the lamp tangentially to its surface S_1 will be transformed, upon reflection at the surface of the elliptical cylinder, to a bundle of rays around the second focal line F_2. The envelope of these rays is a surface S_1', this being the lamp image as formed by the elliptical cylinder. In Fig. 3.4b the particular rays which bound the S_1' surface both horizontally and vertically have been indicated. It is apparent that the image S_1' is elongated in the direction of the minor axis of the elliptical mirror. It can be shown that this image is itself an ellipse. The major and minor axes of this ellipse, R_M and R_m respectively, can then be obtained from Fig. 3.4b by simple geometrical considerations. If we assume that the radius R_L of the lamp is much smaller than the minor axis of the elliptical mirror, we get

$$R_M = R_L\left(\frac{1+e}{1-e}\right) \tag{3.2a}$$

$$R_m = R_L\left(\frac{1-e^2}{1+e^2}\right) \tag{3.2b}$$

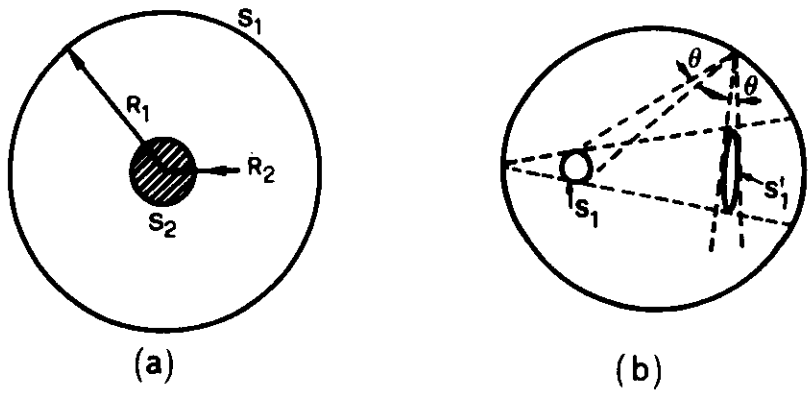

FIG. 3.4. Reduction of the two systems of Fig. 3.2a and b to a single system.

where e is the eccentricity of the elliptical mirror. Now, if this eccentricity is very small, the image S_1' is again a circle of the same radius as that of the lamp. In this case the system of Fig. 3.4b reduces to that of Fig. 3.4a and the surface S_1 of Fig. 3.4a is the surface S_1' of Fig. 3.4b.

Now that the two systems of Fig. 3.2a and b have been reduced to the single system shown in Fig. 3.4a, we can proceed to calculate the fraction of the power emitted by the surface S_1 of Fig. 3.4a which actually enters the surface S_2 of the active rod. To do this we will assume that S_1 can be considered as a blackbody surface at temperature T. According to the Stefan–Boltzmann law, the total power emitted by the lamp is given by

$$P_1 = \sigma_{SB} T^4 S_1 \tag{3.3}$$

where σ_{SB} is the Stefan–Boltzmann constant. The calculation of the power entering the rod then follows from a simple thermodynamic argument.[3] Let us suppose the laser rod is replaced by a blackbody cylinder having the same dimensions as the rod. Obviously, the power P_{2i} entering the surface S_2 will remain the same. Now, if the blackbody cylinder is kept at the same temperature T as the lamp, then, according to the second law of thermodynamics, there will be no net exchange of power between the two blackbody surfaces (lamp and rod). This means that the incident power P_{2i} must equal the power P_{2e} emitted by the rod. Since P_{2e} is given by $P_{2e} = \sigma_{SB} T^4 S_2$, we get

$$P_{2i} = P_{2e} = \sigma_{SB} T^4 S_2 \tag{3.4}$$

Then we readily find from equations (3.3) and (3.4) that the value of the transfer efficiency η_t is given by

$$\eta_t = \frac{P_{2i}}{P_1} = \frac{S_2}{S_1} = \frac{R_2}{R_1} \tag{3.5}$$

where rod and lamp have been assumed to have the same length. The above expression holds provided $R_2 < R_1$. If $R_2 > R_1$ (a situation that obviously can only be achieved with the system of Fig. 3.2b), the transfer efficiency is expected to be always equal to 1. This is, however, rigorously true only when the elliptical pump cavity has zero eccentricity. For finite values of eccentricity, there are calculations available giving the transfer efficiency as a function of the ratio between the lamp and rod diameters.[19] One should also take account of the fact that the reflectivity of the pump cavity is never 100%. In practice, the transfer efficiency of an optimized elliptical cylinder can be as high as 80%. Since the radius R_1 of a helical lamp is usually at least twice the rod radius R_2, the efficiency of a helical lamp is appreciably smaller than that of a linear lamp in an elliptical

reflector. On the other hand, helical lamps provide a more uniform pumping of the laser rod (see the next section) and are often used in high-energy systems when laser beam uniformity is more important than laser efficiency.

3.2.2 Pump Light Distribution

In the previous section we have calculated the fraction of pump light reaching the rod. In this section we want to calculate, for a few representative cases, the distribution of this light within the active rod.

As a first example, we consider the case of a helical flashlamp or, equivalently, that of a very low eccentricity elliptical reflector with lamp diameter larger than the rod diameter. In both of these cases the configuration of Fig. 3.4a applies. We further assume that the lateral surface of the rod is polished. Then, since the refractive index of the rod is usually larger than that of the surrounding medium, the pump light tends to be concentrated toward the rod axis. This can be understood with the help of Fig. 3.5, which shows a rod of radius R and refractive index n surrounded by a medium of unit refractive index. The lamp is not shown. We recall, however, that its radius has been assumed to be equal to (or larger than) R. In this case, the rays falling on point P of the rod surface can arrive from any direction within the angle π shown in Fig. 3.5. The two extreme rays 2 and 3 are indicated in the figure. Upon entering the rod, these rays are refracted and become the rays 2′ and 3′, where the angle θ is the critical

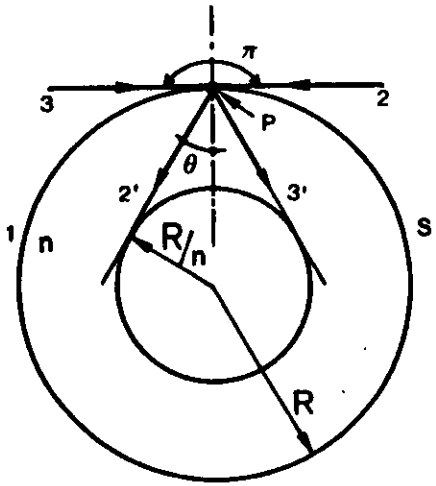

FIG. 3.5. Concentration of rays in a central core of a cylindrical rod, due to refraction.

angle ($\sin\theta = 1/n$). Therefore, all rays arriving from the lamp will be refracted within the angle 2θ between the rays 2′ and 3′. Applying the same argument to all points P of surface S, we arrive at the conclusion that the central core (radius R/n) of the rod is more heavily pumped than the outer part of the rod. The calculation of pump energy density ρ in the rod becomes particularly simple if we make the following assumptions: (i) We only consider light entering the rod in a plane orthogonal to the rod axis and (ii) we neglect the attenuation of this light as it propagates into the rod. In this case the energy density ρ_n at a point within the rod at a distance r from the axis is[4]

$$\rho_n = n^2\rho \qquad (0 < r < R/n) \qquad (3.6a)$$

$$\rho_n = \frac{2n^2}{\pi}\rho \sin^{-1}\left(\frac{R}{nr}\right) \qquad (R/n < r < R) \qquad (3.6b)$$

where ρ is the value that the energy density would have at that same point of the rod if its refractive index were unity. This density is related to the intensity of the light emitted by the lamp by equation (2.19b). If the simplifying assumptions (i) and (ii) are not made, the expression for ρ_n is much more complicated.[5] In Fig. 3.6, computed plots of the dimensionless quantity

$$f(\alpha R, r/R) = \rho_n/n^2\rho \qquad (3.7)$$

are shown for several values of αR, where α is the absorption coefficient at the pump wavelength (the pump light is assumed to be monochromatic). The same figure also shows the predictions of equation (3.6), indicated by a dashed line. Note the difference between the dashed curve and the solid curve corresponding to $\alpha R = 0$. While both curves refer to the case where there is no absorption in the rod, the solid curve, unlike the dashed one, takes account of the fact that light can enter the rod from any direction. Note also that, when $\alpha R \neq 0$, the attenuation of the pump light as it propagates inward from the rod surface tends to smooth out the distribution ρ_n. From the data of Fig. 3.6 it is seen that, at the center of the rod ($r = 0$), the quantity $f(\alpha R, 0)$ can be closely approximated by the expression $f = \exp(-1.1\alpha R)$.

The fact that, for very small values of αR, the energy density in the central region of the rod is $n^2\rho$ deserves some further consideration. Let us assume that the lamp has the same radius as the rod and is placed along the focal axis F_1 of Fig. 3.2b. Since the rays 2 and 3 of Fig. 3.5 are tangent to S, they must have come from two rays which are tangent to the lamp surface. After refraction, rays 2 and 3 become rays 2′ and 3′ which are

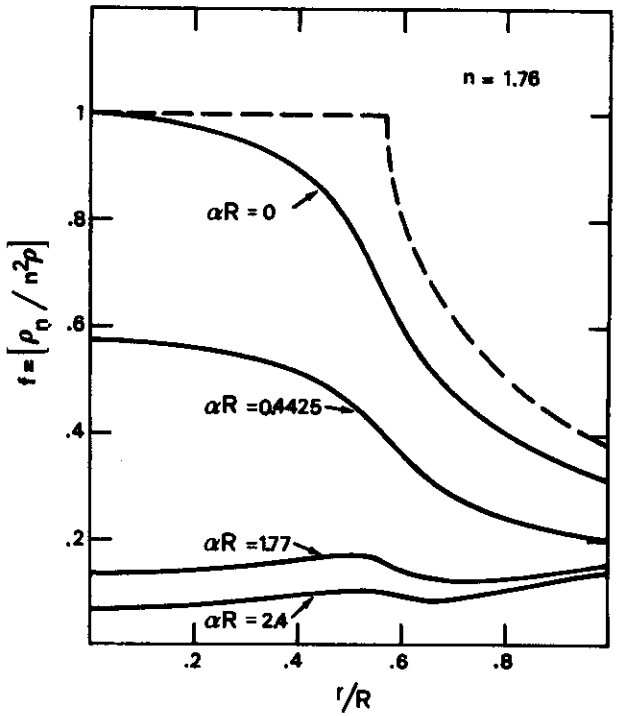

FIG. 3.6. Radial variation of the pump energy density ρ_n for several values of the pump absorption coefficient α (monochromatic pump). The data have been taken from Reference 5.

tangent to a circle of radius R/n. We can, therefore, say that the rod acts like a cylindrical lens in producing an image of the lamp at its center which is n times smaller than the lamp itself. Since the volume of this image is n^2 times smaller than that of the lamp, we can now understand why the corresponding energy density ρ_n is increased by n^2.

We have seen that, for very small values of αR, the pump energy density is uniform only for $r < R/n$, while it is nonuniform outside this central core. A nonuniform energy density is certainly not desirable for an active material. This inconvenience can be overcome[5] by surrounding the active rod by a cylindrical cladding of transparent material with the same refractive index as the rod (Fig. 3.7). In this case, if the radii of both the cladding and the lamp are made equal to nR, we can repeat the argument of Fig. 3.5, starting from a point P of the cladding. The refracted rays 2′ and 3′ will, in this case, be tangent to the surface of the active material, and all the incoming light will be concentrated into the active material. In the

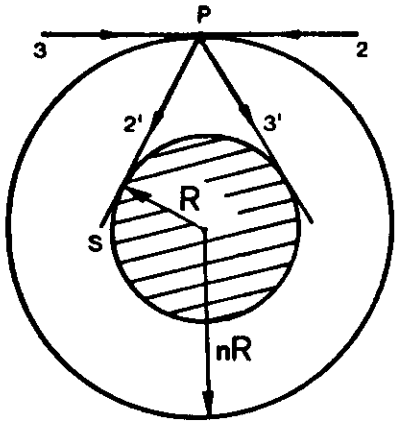

FIG. 3.7. Transparent cylindrical cladding of radius nR to provide a uniform pump density in the active rod (shaded area).

case of $\alpha R = 0$ and for light entering only in the plane of Fig. 3.7, the energy density will now be uniform in the active material and be given by equation (3.6*a*). Another way to provide a more uniform pumping is by grinding the lateral surface of the rod. In this case the pump light, upon entering the rod, will be diffused, and the light concentration shown in Fig. 3.5 will not occur. In Fig. 3.8 computed plots of the dimensionless quantity

$$f_1(\alpha R, r/R) = \rho_n/n\rho \tag{3.8}$$

for several values of αR are shown for this case.[1] Here again α is the absorption coefficient at the pump wavelength (for monochromatic pump light). Note that for $\alpha R = 0$ we have $\rho_n = n\rho$. The factor n arises in this case simply from the fact that the light velocity in the rod is n times smaller than its vacuum value. For a given lamp emission the energy density ρ_n is thus expected to be n times larger than the value ρ which a rod of unit refractive index would produce. From the data of Fig. 3.8 it is seen that, at the center of the rod, $f_1(\alpha R, 0)$ can be closely approximated by the expression $f_1 \simeq \exp(-1.27\alpha R)$. A comparison of (3.8) with (3.7), at $r = 0$, then shows that, apart from the relatively small difference between f and f_1, the pump energy density at the center of the rod is actually reduced by an amount n as a result of roughening the lateral surface. However, the whole cross section of the rod, rather than just the central core of radius R/n, is now more or less uniformly illuminated. In fact it can be shown from Figs. 3.6 and 3.8 that the integrated pump energy density over the rod cross section is approximately the same in the two cases.

We now consider the case where the lamp radius R_L is smaller than the rod radius R_R. We assume the pumping geometry to be that of Fig. 3.2b. If

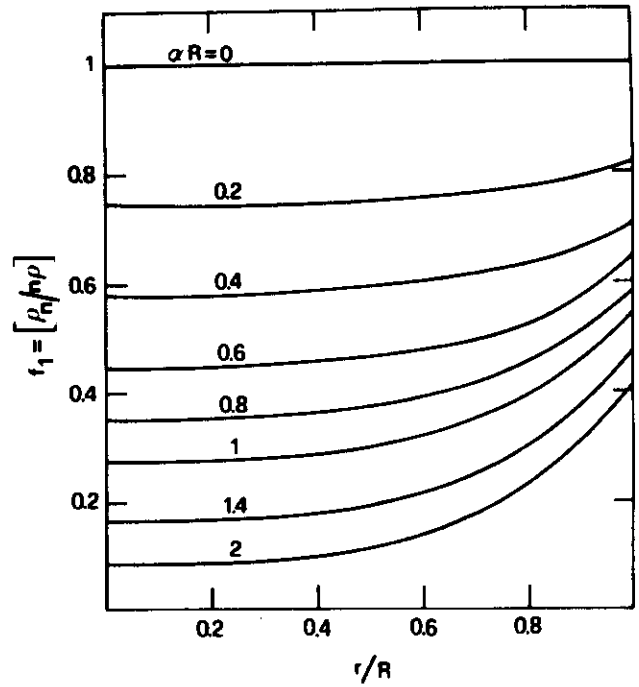

FIG. 3.8. Rod with rough-ground lateral surface. Radial variation of the normalized pump energy density ($\rho_n/n\rho$) versus normalized radius (r/R) for several values of the pump absorption coefficient α (after Reference 1).

the rod lateral surface is polished, an elliptical image of the lamp will be formed in the rod (see Fig. 3.4b). Due to refraction at the rod surface, the major and minor axes of this image are both reduced by a factor n from the values given in expressions (3.2*a*) and (3.2*b*). To avoid this nonuniform pump distribution, the rod lateral surface can again be rough ground.

So far, the discussion applies to monochromatic pump radiation. For polychromatic radiation, the same relations as in (3.6) to (3.8) apply and so also do the curves of Figs. 3.6 and 3.8 provided, however, that ρ_n and ρ are replaced by the spectral quantities $\rho_{n\lambda}$ and ρ_λ.

3.2.3 *Pumping Rate*[6]

Let us first consider a monochromatic pump of frequency ω. The pump power absorbed per unit volume of the rod, dP/dV, is then given by

$$\frac{dP}{dV} = WN_g\hbar\omega \tag{3.9}$$

where W is the absorption rate and the upper pump level has been assumed empty. With the help of (2.53c) and (2.61), equation (3.9) can be written as

$$\frac{dP}{dV} = \frac{c_0}{n}\sigma N_g \rho_n \tag{3.10}$$

where ρ_n is the pump energy density at the point in question. For polychromatic pump radiation, (3.10) can be written in terms of the corresponding spectrally dependent variables, *viz.*,

$$\frac{dP_\lambda}{dV} = \frac{c_0}{n}\sigma N_g \rho_{n\lambda} \tag{3.10a}$$

where P_λ is such that $(dP_\lambda/dV)d\lambda$ is the power absorbed per unit volume from pump radiation with wavelength lying between λ and $\lambda + d\lambda$.

As a particularly relevant example, we now consider the case in which the lateral surface of the rod is rough ground. With the help of (3.8) and (2.19c), equation (3.10a) can be written as

$$\frac{dP_\lambda}{dV} = 4\eta_t \sigma N_g f_1 I_\lambda \tag{3.11}$$

where η_t is the transfer efficiency of the given pump configuration. The rate at which the upper state becomes populated by the pumping process is then

$$\frac{dN_2}{dt} = \int \eta_q \frac{1}{\hbar\omega}\frac{dP_\lambda}{dV}\,d\lambda$$

$$= 4\eta_t N_g \int \frac{\eta_q \sigma f_1}{\hbar\omega} I_\lambda\, d\lambda \tag{3.12}$$

where $\eta_q = \eta_q(\lambda)$ is the pump quantum efficiency. A comparison of (3.12) with (1.10) then gives

$$W_p = 4\eta_t \int \frac{\eta_q \sigma f_1}{\hbar\omega} I_\lambda\, d\lambda \tag{3.13}$$

With the help of (3.2), we can re-express Eq. (3.13) more conveniently as

$$W_p = 4\eta_t \eta_r \frac{P}{2\pi R l} \int \frac{\eta_q \sigma f_1}{\hbar\omega} g_\lambda\, d\lambda \tag{3.14}$$

Note that, according to (3.7), the right-hand side of (3.13) and (3.14) should be multiplied by n, and f_1 replaced by f, in the case of a rod with a polished surface.

Equations (3.13) and (3.14) are the desired expressions for the pump rate. They depend on the properties of the active material [quantum efficiency $\eta_q(\lambda)$ and absorption cross section $\sigma(\lambda)$ of the pump bands] and on the spectral emission of the lamp (I_λ or g_λ). Since $f_1 = f_1(\alpha R, r/R)$, it follows that W_p will also depend on the concentration of active ions, on the rod radius R, and on the normalized radial coordinate r/R. A calculation

TABLE 3.1. Efficiency Terms for Optical Pumping (%)

Case	η_t	η_r	η_a	η_{pq}	η_p
1	30–40	25	30–60	50	1.1–3
2	80	50	16	40	2.6

of W_p therefore requires knowledge of all these quantities. To simplify matters, an overall pumping efficiency η_p is sometimes introduced. This is defined as the ratio of the minimum possible power required to produce a given pumping in the rod (i.e., $\langle W_p\rangle N_g V\hbar\omega_0$, where $\langle W_p\rangle$ is the average value of W_p over the rod volume V, and ω_0 is the frequency of laser transition) to the actual electrical power input, P, to the lamp required to produce this pumping. Therefore we can write

$$\langle W_p\rangle = \eta_p \frac{P}{V N_g \hbar\omega_0} \tag{3.15}$$

The pump efficiency η_p can be split up into the product of four terms[7]: (i) the transfer efficiency η_t; (ii) the lamp radiative efficiency η_r; (iii) the absorption efficiency η_a which gives the fraction of the useful radiation which is actually absorbed by the rod; (iv) the power quantum efficiency η_{pq}, which is that fraction of the absorbed power which leads to population of the laser level. Notice that this last quantity is similar to the pump quantum efficiency η_q defined previously. Estimates for these efficiency factors defined above are available in the literature.[7] Table 3.1 gives these values for a 6.3-mm-diameter ruby rod pumped by a xenon helical flashtube (Case 1) and for a 6.3-mm-diameter Nd^{3+}:YAG rod pumped by a Kr lamp (Case 2). It must be stressed, however, that the values given in the table are only rough estimates, and an accurate calculation of W_p at each point of the rod can only be obtained through Eq. (3.14).

3.3 *ELECTRICAL PUMPING*[8,9]

This type of pumping is used for gas and semiconductor lasers. We will limit ourselves here to a discussion of the electrical pumping of gas lasers. In this case pumping is achieved by allowing a current of suitable value to pass through the gas. Ions and free electrons are produced, and since they are accelerated by the electric field, they acquire additional kinetic energy and are able to excite a neutral atom by collision. For this impact excitation, the movement of the ions is usually less important than that of the electrons. For a low-pressure gas, in fact, the average electron energy is

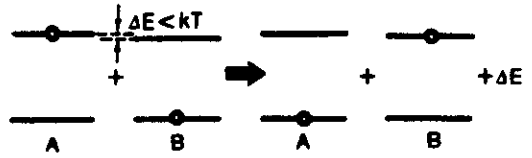

FIG. 3.9. Near-resonant energy transfer between two atoms (or molecules) A and B.

much greater than the corresponding ion energy. After a short time, an equilibrium condition is established among the electrons, and this can be described by an effective electron temperature T_e.

Electrical pumping of a gas usually occurs via one of the following two processes: (i) For a gas consisting of only one species, the excitation can only be produced by electron impact, i.e., according to the process

$$e + X \rightarrow X^* + e \tag{3.16}$$

where X and X^* represent the atom in the ground and excited states, respectively. Such a process is called a collision of the *first kind*. (ii) For a gas consisting of two species (say A and B), excitation can also occur as a result of collisions between atoms of different species through a process known as *resonant energy transfer*. With reference to Fig. 3.9, let us assume that species A is in the excited state and species B in the ground state. We will also assume that the energy difference ΔE between the two transitions is less than kT. In this case, there is an appreciable probability that, after the collision, species A will be found in its ground state and species B in its excited state. The process can be denoted by

$$A^* + B \rightarrow A + B^* + \Delta E \tag{3.17}$$

where the energy difference ΔE will be added to or subtracted from the translational energy, depending on its sign. This process provides a particularly attractive way of pumping species B, if the upper state of A is metastable (forbidden transition). In this case, once A is excited to its upper level by electron impact, it will remain there for a long time, thus constituting an energy reservoir for excitation of the B species. A process of the type indicated in (3.17) is called a collision of the *second kind*.†

†Collisions of the *first kind* involve conversion of the kinetic energy of one species into potential energy of another species. In collisions of the *second kind*, potential energy is converted into some other form of energy (other than radiation) such as kinetic energy, or is transferred as potential energy (in the form of electronic, vibrational, or rotational energy) to another like or unlike species. Collisions of the second kind therefore include not only the reverse of collisions of the first kind (e.g., $e + X^* \rightarrow e + X$) but also, for instance, the conversion of excitation energy into chemical energy.

3.3.1 Electron Impact Excitation[10]

Electron impacts can involve both elastic and inelastic collisions. In an inelastic collision, the atom may either be excited to a higher state or be ionized. All three of these phenomena take place in an electrical discharge and influence its behavior in a complicated way.

For the sake of simplicity, let us first consider the case of impact excitation by a beam of collimated monoenergetic electrons. If F_e is the electron flux (electrons/cm^{2}sec), a total collision cross section σ_e can be defined in a similar way to the case of a photon flux [see equation (2.62)], namely,

$$dF_e = -\sigma_e N_g F_e \, dz \tag{3.18}$$

Here dF_e is the change of flux which takes place when the beam propagates a distance dz in the material. Collisions which produce electronic excitation will only account for some fraction of this total cross section. If we let σ_{e2} be the cross section for electronic excitation from the ground level to the upper laser level, then, according to (3.18), the rate of population of the upper state due to the pumping process is

$$(dN_2/dt)_p = \sigma_{e2} N_g F_e = N_g N_e v \sigma_{e2} \tag{3.19}$$

where v is the electron velocity and N_e is the electron density. A calculation of the pump rate requires a knowledge of the σ_{e2} value in addition to information about the e-beam parameters. This quantity σ_{e2} is in turn a function of the e-beam energy E (i.e., of v), and its qualitative behavior is sketched in Fig. 3.10. Note that there is a threshhold E_{th} for the process to occur and that this threshhold is approximately equal to the energy which is required for the $0 \rightarrow 2$ atomic transition. The cross section σ then reaches a maximum value (at an energy which may be a few electron volts higher than E_{th}) and decreases thereafter. The peak value of σ and the width of the $\sigma = \sigma(E)$ curve depend on the type of transition. The simplest calculation for electron-impact cross section is made using the Born approximation. The basic assumption here is that there is only a weak electrostatic interaction between the incident electron [which is described by the wave function $\exp(i\mathbf{k}_0 \cdot \mathbf{r})$] and the electrons of the atom, so that the chance of a transition occurring in the atom during impact is very small and the chance of two such transitions may be neglected. In this case the Schrödinger equation for the problem can be linearized. The transition cross section involves a factor of the form $\int u_n^* \exp i[(\mathbf{k}_0 - \mathbf{k}_n) \cdot \mathbf{r}] u_0 \, dV$, where u_0 and u_n are the wavefunctions of the ground and excited states respectively, and $\mathbf{k}_n$ is the wavevector of the scattered electron. It is further assumed that the electron wavelength $\lambda = 2\pi/k_0$ is appreciably larger than the size of the

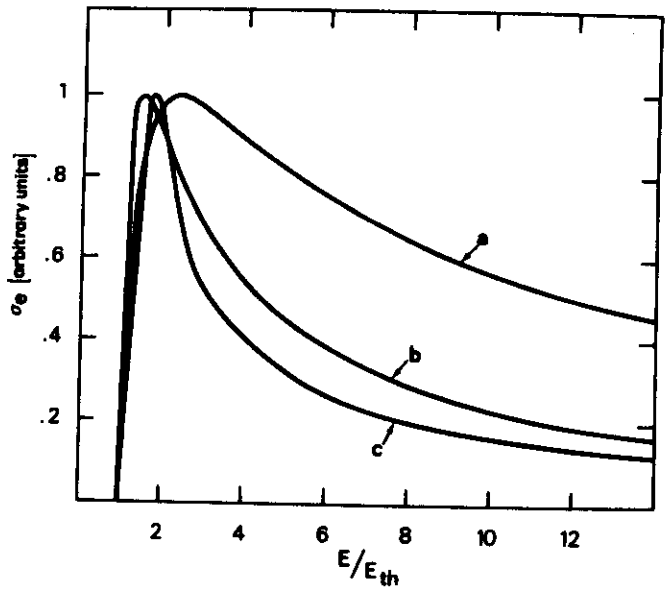

FIG. 3.10. Qualitative behavior of electron-impact excitation cross section versus the energy of the incident electron: (a) optically allowed transition; (b) optically forbidden transition involving no change of multiplicity; (c) optically forbidden transition involving a change of multiplicity. Curves a, b, and c have been derived from those given in Reference 12 for $2p$ and $2s$ transitions in H and 2^3S transition in He, respectively.

atom [$\lambda = (12.26/V)\,\text{Å}$, where V is the electron energy in electron volts]. In this case the factor $\exp i[(\mathbf{k}_0 - \mathbf{k}_n)\cdot\mathbf{r}]$ appearing in the above integral can be expanded in a power series about the atom position. One can distinguish three general types of electron impact depending on the type of transition involved: (i) optically allowed transitions; (ii) optically forbidden transitions involving no change of multiplicity; (iii) transitions involving a change of multiplicity.

For optically allowed transitions, we retain only the first nonvanishing term in the expression of $\exp i(\mathbf{k}\cdot\mathbf{r})$ (i.e., $i\mathbf{k}\cdot\mathbf{r}$, where $\mathbf{k} = \mathbf{k}_0 - \mathbf{k}_n$) and this leads to a cross section of the form

$$\sigma_e \propto |\mu|^2 g(E) \tag{3.20}$$

where $|\mu|^2$ is given by (2.43) and $g(E)$ is a function of the electron energy. For an optically allowed transition, the electron impact cross section σ_e is seen to depend on the same matrix element $|\mu|$ which occurs in the expression for the photon absorption cross section. The transition probability for electron impact is thus proportional to the corresponding photon absorption probability. The quantity $g(E)$ turns out to be a relatively

slowly varying function of E. The decreasing part of the corresponding $\sigma(E)$ curve in Fig. 3.10 varies as $E^{-1}\ln E$ and the width of the curve may be typically 10 times larger than the threshold energy E_{th} (Fig. 3.10a). The peak value of σ is typically 10^{-16}cm^2.

For optically forbidden transitions involving no change in multiplicity ($\Delta S = 0$, e.g., $1^1S \rightarrow 2^1S$ transition in He, see Fig. 6.4), the Born approximation gives a nonvanishing cross section for the next-higher-order term in the expansion of $\exp i(\mathbf{k}\cdot\mathbf{r})$. The corresponding cross section σ_e can again be expressed as in (3.20). The quantity $|\mu|^2$ is now given by $|e\int u_2^* x^2 u_1\,dx|^2$ rather than $|e\int u_2^* x u_1\,dx|^2$, which of course is zero. The rate of fall of the $g(E)$ curve is somewhat faster than in the previous case, the curve behaving as E^{-1} rather than $E^{-1}\ln E$. Peak values of σ are typically of the order of 10^{-19}cm^2 and the width of the curve now may be only 3–4 times larger than the threshold energy E_{th} (Fig. 3.10b).

When a change of multiplicity is involved (e.g., $1^1S \rightarrow 2^3S$ in He, Fig. 6.4) the Born approximation gives a zero cross section in any order of expansion of $\exp(i\mathbf{k}\cdot\mathbf{r})$. In fact, such a transition involves a spin change while, within the Born approximation, the incoming electron only couples to the orbital motion of the atom.† It must be remembered, however, that it is the total spin of the atom plus the incident electron which must be conserved, not necessarily that of the atom alone. Transitions may, therefore, occur via electron *exchange* collisions, wherein the incoming electron replaces the electron of the atom involved in the transition and this electron is in turn ejected by the atom (during the collision, however, the two electrons are quantum mechanically indistinguishable). To conserve spin, the incoming electron must have its spin opposite to that of the ejected one. The peak cross section for this type of transition is usually fairly high ($\sim 10^{-16}\text{cm}^2$). The cross section rises very sharply at threshold and falls off rapidly thereafter. The width of the curve may now be typically equal to or smaller than the value of the threshold energy (Fig. 3.10c).

The discussion so far applies to a monoenergetic beam of electrons. In a gas discharge, however, the electrons will not be monoenergetic but will instead have some particular energy distribution $f(E)$[$f(E)\,dE$ is the probability for an electron to have its energy lying between E and $E + dE$]. In this case the rate of population of the upper state is obtained from (3.19) by averaging over this distribution, *viz.*,

$$\left(\frac{dN_2}{dt}\right)_p = N_g N_e \langle v\sigma_{e2}\rangle \tag{3.21}$$

†This assumes a negligible spin–orbit coupling, which is true for light atoms (e.g., He, Ne) while it is not true for heavy atoms like Hg.

where

$$\langle v\sigma \rangle = \int v\sigma(E) f(E)\, dE \tag{3.22}$$

If a Maxwellian energy distribution is assumed then $f(E) \propto E^{1/2} \cdot \exp[-(E/kT_e)]$, and the only quantity which needs to be known is the electron temperature T_e. This can be related to the applied electric field $\mathcal{E}$ provided we make the assumption that, at each collision, some fraction δ of the kinetic energy of the electron is lost. If v_{th} is the average thermal electron velocity, the average kinetic energy is about $mv_{th}^2/2$. The collision rate is v_{th}/l, where l is the electron mean free path. The power lost by the electron is therefore $\delta(v_{th}/l)(mv_{th}^2/2)$, and this must be equal to the power delivered by the electric field, which is $e\mathcal{E}v_{drift}$. Since the drift velocity v_{drift} is in turn given by $el\mathcal{E}/mv_{th}$, the power delivered by the electric field is $e^2l\mathcal{E}^2/mv_{th}$. By equating the two above expressions we finally get the following expression for the electron temperature ($T_e = mv_{th}^2/2k$), *viz.*,

$$T_e = \frac{e}{(2\delta)^{1/2}k}(\mathcal{E}l) \tag{3.23}$$

Since the mean free path l is inversely proportional to the gas pressure p, (3.23) shows that, for a given gas, T_e depends solely on the $\mathcal{E}/p$ ratio. This ratio is the fundamental quantity involved in establishing a given electron temperature, and it is often used in practice as a useful parameter for specifying the discharge conditions. For a given gas mixture there generally exists some value of the $\mathcal{E}/p$ ratio which maximizes the pump rate. Too low a value of $\mathcal{E}/p$ results in too low a value of the electron temperature T_e to excite the laser pump levels effectively. Conversely, too high a value of $\mathcal{E}/p$ (i.e., of T_e) leads to excitation of higher levels of the gas mixture (which may not be so strongly coupled to the laser transition) and to excessive ionization of the gas mixture (which may result in a discharge instability, i.e., a transition from a glow discharge to an arc).

According to (1.10) and (3.21) the pump rate W_p is

$$W_p = N_e\langle v\sigma \rangle \tag{3.24}$$

where $\langle v\sigma \rangle$ is given by (3.22), the electron temperature being expressed through (3.23) as a function of the applied field $\mathcal{E}$. The electron density N_e can then be expressed as a function of the current density J and the drift velocity v_{drift} as

$$N_e = J/ev_{drift} \tag{3.24a}$$

According to the previous calculation v_{drift} can be written as

$$v_{drift} = \frac{el\mathcal{E}}{mv_{th}} = \left(\frac{\delta}{2}\right)^{1/4}\left(\frac{el\mathcal{E}}{m}\right)^{1/2} \tag{3.24b}$$

From (3.24), with the help of (3.24*a*) and (3.24*b*) we obtain

$$W_p = \frac{J}{c}\left[\langle v\sigma \rangle\left(\frac{2}{\delta}\right)^{1/4}\left(\frac{m}{el\mathcal{E}}\right)^{1/2}\right] \tag{3.24c}$$

and the expression in the square brackets depends only on the product $l\mathcal{E}$, i.e., on the $\mathcal{E}/p$ ratio. Since this ratio is generally kept at its optimum value, a change in pump rate is achieved by changing the current density J in the gas discharge.

The calculation given above is a rather crude one since it is based on the assumption of a Maxwellian distribution which in fact is not found to hold in practice.[11] For neutral atom and ion gas lasers, however, the departure from a Maxwellian distribution is not so great and this distribution is therefore often used. However, in molecular gas lasers oscillating on vibrational transitions, the gas is usually weakly ionized and the mean electron energy is low ($E \simeq 1$ eV, since only vibrational states need to be excited) in comparison with that (10–30 eV) needed for neutral atom and ion gas lasers. Accordingly, the assumption of a Maxwellian distribution is expected to be inadequate for molecular lasers. One needs in this case to carry out an *ab initio* calculation to obtain the electron energy distribution $f(E)$. This is done using the appropriate electron transport equation (the Boltzmann equation), and it requires a knowledge of all possible electron collision processes leading to excitation (or de-excitation) of the vibrational or electronic levels of all gas species in the discharge. The calculation therefore gets quite involved, and sometimes it may be impracticable because of the lack of appropriate data on electron collision cross sections. Detailed computer calculations have therefore only been performed for gas mixtures of particular importance such as the CO_2–N_2–He mixture used in high-power CO_2 lasers.[12,13] These calculations do indeed show a considerable departure from a Maxwellian distribution. However, the average electron temperature and the overall excitation rates still turn out to be, for a given gas mixture, a function only of the $(\mathcal{E}/p)$ ratio, as indeed indicated by our crude calculation.

3.3.2 Spatial Distribution of the Pump Rate

In the positive column of a glow discharge the dc electric field, hence the drift velocity v_{drift}, are independent of the discharge current J. It then follows that the spatial dependence of the electron density N_e[see (3.24*a*)], hence of the pump rate W_p [see (3.24)], is the same as that of the current density J.

In the situation where the gas is contained in a cylindrical tube and the discharge current is flowing along the tube, the radial dependence of J can be analytically specified.[14, 15] For both neutral atom and ion gas lasers, electron–ion recombination can be assumed to occur only at the walls.† Thus, if the ion mean free path is much shorter than the tube radius R, recombination occurs by ambipolar diffusion to the walls. In this case one can apply the Schottky theory for a gas positive column, and the radial distribution of the discharge electrons is predicted to vary as $J_0(2.4r/R)$ where J_0 is the Bessel function of zeroth order. This function is plotted in Fig. 3.11. Note that the electron density drops to zero at the tube walls. Note also that an ion balance equation can be obtained using the condition that the rate of electron–ion pair production must equal the rate of electron–ion pair recombination at the tube walls. This equation leads to a relation between the electron temperature‡ T_e (whose value establishes the ionization rate) and the product pR (whose value, via diffusion, establishes the recombination rate). Accordingly, for a given gas, T_e turns out to be a function of pR only. The ion balance equation thus leads to a relation between T_e and pR in much the same way as the energy balance equation leads to a relation between T_e and $\mathcal{E}/p$ [see (3.23)]. Experimental results have shown that the Schottky theory does hold for noble gas lasers involving neutral atoms and for high-pressure noble gas ion lasers. It is also interesting to note that a Bessel-like radial behavior of the electron density in the discharge has also been used to give accurate predictions of the radial distribution of inversion in a CO_2 laser.[16]

When the ion mean free path becomes comparable with the tube radius (as happens in the relatively low-pressure ion gas lasers), electrons and ions reach the walls by free flight rather than by diffusion. In this case one should use the "free-fall" model of Tonks–Langmuir for the plasma discharge.[17] In this case the radial distribution of the discharge electrons, although no longer given by a Bessel function, still has a bell-shaped form (Fig. 3.11). Note also that the ion balance equation again leads to a relation between the electron temperature and the pR product.

When the gas is excited by a current flowing transversely to the resonator axis (as, for example, with two electrodes placed along the resonator axis, see Fig. 6.15) a reliable prediction of the spatial distribution of the pump rate becomes difficult. In fact the distribution is affected by

†Ion–electron ($e + A_i$) recombination within the discharge volume is an unlikely process since it would require the recombination energy to be removed (radiatively) within the short duration of the collision. A three-body process $e + A_i + M$ where the excess energy is given to the third partner, M, is also unlikely at the gas pressure used (a few Torr).

‡A Maxwellian distribution is assumed in the Schottky theory.

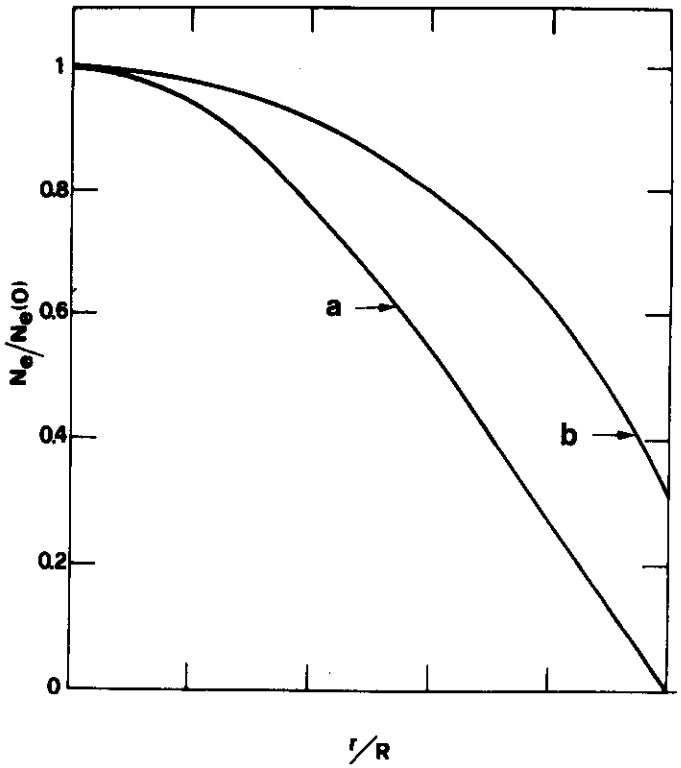

FIG. 3.11. Radial behavior of the electron density for a gas contained in a cylindrical tube (longitudinal discharge): (a) Schottky theory (high-pressure gas); (b) Tonks–Langmuir theory (low-pressure gas).

the shape of the electrodes, by the type and geometry of the auxiliary ionizing sources which are sometimes used, and by the flow conditions of the gas mixture in the discharge chamber. Experimental measurements of the resulting population inversion have indicated a rather nonuniform and asymmetric pump distribution for this type of discharge (a 50% variation of pump rate from center to periphery of the discharge channel may typically be observed).

3.3.3 *Pumping Efficiency*

As we have seen from the preceding discussion, the electrical pumping of gas lasers is a very complicated process, and a closed expression for the pump rate (such as that obtained for the optical pumping case) cannot, in general, be given. Just as in the optical pumping case, however, we can again define an overall pumping efficiency η_p as the ratio between the

minimum power required to produce a given inversion (i.e., $\langle W_p \rangle N_g V \hbar\omega_p$, where $\langle W_p \rangle$ is the average value of W_p over the discharge volume V, and $\hbar\omega_p$ is the energy of the upper laser level) and the electrical power input P to the discharge. Therefore we can write

$$\langle W_p \rangle = \eta_p \frac{P}{V N_g \hbar\omega_p} \tag{3.25}$$

Note that it has been assumed that only one pump level (of energy $\hbar\omega_p$) plays a role, and η_p has therefore been defined in a slightly different way from that for the case of optical pumping [compare (3.25) with (3.15)]. Calculations of η_p are available in the literature for a few gas mixtures of notable interest. In particular, for a CO_2:N_2:He (1:1:8) gas mixture and for an average electron energy of 1 eV, η_p may be as high as 70%.[12, 18]

3.3.4 Excitation by (Near) Resonant Energy Transfer[8,10]

In this case, too, the phenomenon can be described by a suitable collision cross section σ_{AB}:

$$\left(\frac{dN}{dt}\right)_{AB} = N_A N_B v \sigma_{AB} \tag{3.26}$$

where $(dN/dt)_{AB}$ is the number of transitions per unit volume per unit time for the process (3.17), N_A is the upper state population of atoms A, N_B is the lower state population of atoms B, and v is the (relative) velocity of the two atoms. For a gas at temperature T, the quantity $v\sigma_{AB}$ must be averaged over the velocity distribution.

The behavior of σ_{AB} versus the energy defect ΔE between the two levels deserves some comment. Since we are dealing with a resonant process we would expect $\sigma_{AB}(\Delta E)$ to be a sharply peaked function of ΔE, with the maximum obviously occurring at $\Delta E = 0$. In this excitation process, what actually occurs physically is as follows: When atom A approaches atom B, the latter will be subjected to a potential energy of either attractive (see Fig. 2.22) or repulsive (see Fig. 6.21) type. We shall denote this potential by $U(\mathbf{r}, \mathbf{R})$ where $\mathbf{r}$ refers to the electron coordinates and $\mathbf{R}$ the nuclear coordinates of the two-atom system (see also section 2.9.3). The relative motion of the two atoms [i.e., $\mathbf{R} = \mathbf{R}(t)$] therefore produces a time-varying potential $U(\mathbf{r}, t)$.† This term will act as a time-dependent Hamiltonian $\mathcal{H}_u(\mathbf{r}, t)$ which couples together the translational and internal motions of

†Note that, when the two colliding species are atoms, the only nuclear coordinate of interest is the internuclear distance. When, however, the colliding species are molecules, the interaction potential will also depend on the mutual orientation of the two molecules.

the two-atom system. A time-dependent perturbation analysis shows[8] that the transition cross section σ_{AB} can be written as

$$\sigma_{AB} \propto \left| \int_{-\infty}^{+\infty} H'_u(t) \exp(i\omega_{if} t)\, dt \right|^2 \tag{3.27}$$

where $H'_u(t) = \int \psi_f^*(\mathbf{r}) \mathcal{H}_u(\mathbf{r}, t) \psi_i(\mathbf{r})\, d\mathbf{r}$ is the transition matrix element between the initial state ψ_i [species A in the excited state and B in the gound state] and the final state ψ_f [species A in the ground state and B in the excited state]. In equation (3.27) ω_{if} is given by $\omega_{if} = \Delta E/\hbar$, where ΔE is the energy defect of the resonant process (see Fig. 3.9). The energy transfer cross section σ_{AB} is thus proportional to the power spectrum $|H_u(\omega_{if})|^2$ of the matrix element $H'_u(t)$ at the frequency $\Delta E/\hbar$. We can therefore say that σ_{AB} is established by the Fourier transform $U(\mathbf{r}, \omega)$ of the time-varying potential $U(\mathbf{r}, t)$ at the frequency ω_{if} required to induce the transition. Since $U(\mathbf{r}, t)$ is expected to be nonzero only for a time of the order of the collision duration $\Delta\tau_c$ [given by (2.101)], its Fourier transform is expected to have a bandwidth of the order of $1/\Delta\tau_c$. More precisely, for binary collisions, the frequency behavior of both $|H'_u(\nu)|^2$ and σ_{AB} can be shown to be of the form $\exp(-\nu\Delta\tau_c)$. Thus σ_{AB} is resonantly large over a range ΔE_r of the energy defect ΔE, given by

$$\Delta E_r = \frac{h}{\Delta\tau_c} \tag{3.28}$$

In the case of Ne one has $\Delta\tau_c \simeq 10^{-13}$ s [see (2.103)], and from (3.28) we find $\Delta E_r = 0.006$ eV. Note that this value is appreciably smaller than $kT (\simeq 0.025$ eV at room temperature). For an energy defect ΔE less than ΔE_r, σ_{AB} may be as large as $10^{-14}\,\text{cm}^2$. Therefore near-resonant collisions provide a very convenient way of selectively populating a given transition.

PROBLEMS

3.1 A ruby rod with 6.3 mm diameter is pumped by a helical flashlamp of ~2 cm diameter. Calculate the pump transfer efficiency.

3.2 A laser rod in an elliptical pumping chamber has rough ground sides in order to achieve a uniform pump distribution. The flashlamp and rod diameters are assumed equal. Let I_λ be the lamp spectral intensity, S the lateral surface, and V the volume of the active material. By considering only radially propagating rays, show that the (average) pump rate is

$$W_p = \frac{\eta_t}{N_g V} \int \eta_q (1 - e^{-2\alpha R}) \frac{S I_\lambda\, d\lambda}{\hbar\omega}$$
$$= \frac{S\eta_t}{N_g V} \int \eta_q [e^{\alpha R} - e^{-\alpha R}] e^{-\alpha R} \frac{I_\lambda\, d\lambda}{\hbar\omega}$$

Show that, if we assume $\exp(\alpha R) - \exp(-\alpha R) \simeq 2\alpha R$ and $\exp(-\alpha R) \simeq f_1$, the above expression reduces to (3.13).

3.3 Using (3.14) and (3.15) show that $\eta_p = 2\eta_i\eta_r \int \eta_q \alpha R \langle f_1 \rangle (\lambda/\lambda_0) g_\lambda \, d\lambda$, where $\langle f_1 \rangle$ is the average of f_1 over the rod cross section.

3.4 Show that the power quantum efficiency η_{pq} is given by

$$\eta_{pq} = \frac{\int W_p N_g \hbar\omega_0 \, dV}{\int (dP_\lambda/dV) \, d\lambda \, dV}$$

where the volume integrals are taken over the rod volume. With the help of (3.11), (3.14), and (3.2) show that

$$\eta_{pq} = \frac{\int\int \eta_q \sigma \langle f_1 \rangle (\lambda/\lambda_0) g_\lambda \, d\lambda}{\int \sigma \langle f_1 \rangle g_\lambda \, d\lambda}$$

where $\langle f_1 \rangle$ is the average of f_1 over the rod cross section.

3.5 Using the results obtained in Problems 3.3 and 3.4, show that $\eta_p = \eta_i \eta_r \eta_{pq} \eta_a$, where the absorption efficiency η_a is given by

$$\eta_a = 2 \int \alpha R \langle f_1 \rangle g_\lambda \, d\lambda$$

3.6 For radially propagating rays, using the expression for W_p given in Problem 3.2, show that $\eta_{pq} = \int \eta_q h(\lambda)(\lambda/\lambda_0) g_\lambda \, d\lambda / \int h(\lambda) g_\lambda \, d\lambda$ and $\eta_a = \int h(\lambda) g_\lambda \, d\lambda$, where $h(\lambda) = 1 - \exp(-2\alpha R)$.

3.7 With the help of Fig. 3.8 calculate $\langle f_1 \rangle$ for each value of αR.

REFERENCES

1. W. Koechner, *Solid-State Laser Engineering* (Springer-Verlag, New York, 1976), Chapter 6, Springer Series in Optical Sciences, Vol. 1.
2. D. Ross, *Lasers, Light Amplifiers, and Oscillators* (Academic Press, New York, 1969), Chapter 14.
3. O. Svelto, *Appl. Opt.* 1, 745 (1962).
4. G. E. Devlin, J. McKenna, A. D. May, and A. L. Schawlow, *Appl. Opt.* 1, 11 (1962).
5. C. H. Cooke, J. McKenna, and J. R. Skinner, *Appl. Opt.* 3, 957 (1964).
6. W. Kaiser, C. G. B. Garret, and D. L. Wood, *Phys. Rev.* 123, 766 (1961).
7. W. Koechner, *Solid-State Laser Engineering* (Springer-Verlag, New York, 1976), pp. 85, 105, and 324.
8. C. K. Rhodes and A. Szoke, "Gaseous Lasers: Atomic, Molecular and Ionic," in *Laser Handbook*, ed. by F. T. Arecchi and E. O. Schultz-Dubois (North-Holland Publishing Co., Amsterdam, 1972), Vol. I, pp. 265–324.
9. C. S. Willett, *An Introduction to Gas Lasers: Population Inversion Mechanisms* (Pergamon Press, Oxford, 1974).
10. H. S. W. Massey and E. H. S. Burhop, *Electronic and Ionic Impact Phenomena* (Oxford University Press, London, 1969), Vols. I and II.

11. C. S. Willett, *An Introduction to Gas Lasers: Population Inversion Mechanisms* (Pergamon Press, Oxford, 1974), pp. 84, 280, and 327.
12. W. L. Nighan, *Phys. Rev. A* 2, 1989 (1970).
13. K. Smith and R. M. Thomson, *Computer Modeling of Gas Lasers* (Plenum Press, New York, 1978).
14. C. E. Webb, in *High-Power Gas Lasers*, ed. by E. R. Pike (The Institute of Physics, Bristol, 1976), pp. 1–28.
15. C. S. Willet, *An Introduction to Gas Lasers: Population Inversion Mechanisms* (Pergamon Press, Oxford, 1974), Section 3.2.2.
16. P. K. Cheo, in *Lasers*, ed. by A. K. Levine and A. J. DeMaria (Marcel Dekker, New York, 1971), Chapter 2.
17. C. C. Davis and T. A. King, in *Advances in Quantum Electronics*, ed. by D. W. Goodwin (Academic Press, New York, 1975), pp. 170–437.
18. A. J. DeMaria, in *Principles of Laser Plasmas*, ed. by G. Bekefi (Wiley-Interscience, Inc., New York, 1976), Chapter 8.
19. C. Bowness, *Appl. Opt.* 4, 103 (1965).

(13)